Computers and Concrete, Vol. 11, No. 4 (2013) 351-364
DOI: http://dx.doi.org/10.12989/cac.2013.11.4.351

Analysis of steel-GFRP reinforced concrete circular columns

M.S. Shraideh and R.S. Aboutaha*

Civil and Environmental Engineering, Syracuse University, Syracuse, USA

(Received April 16, 2012, Revised October 4, 2012, Accepted October 19, 2012)

Abstract. This paper presents results from an analytical investigation of the behavior of steel reinforced concrete circular column sections with additional Glass Fiber Reinforced Polymers (GFRP) bars. The primary application of this composite section is to relocate the plastic hinge region from the column-footing joint where repair is difficult and expensive. Mainly, the study focuses on the development of the full nominal moment-axial load (M-P) interaction diagrams for hybrid concrete sections, reinforced with steel bars as primary reinforcement, and GFRP as auxiliary control bars. A large parametric study of circular steel reinforced concrete members were undertaken using a purpose-built MATLAB© code. The parameters considered were amount, location, dimensions and mechanical properties of steel, GFRP and concrete. The results indicate that the plastic hinge was indeed shifted to a less critical and congested region, thus facilitating cost-effective repair. Moreover, the reinforced concrete steel -GFRP section exhibited high strength and good ductility.

Keywords: reinforced concrete; bridge columns and foundations; material constitutive models; glass fiber reinforced polymers (GFRP); plastic hinge

1. Introduction

A composite section is defined as a structural member constructed of two or more dissimilar materials attached together to work as one unit and to make the best use of the different material response features. Steel-concrete composite sections are among the most widely used types of composite systems in construction. Steel members have advantages of high tensile strength and ductility, while concrete members have advantages in compressive strength and stiffness as well as high fire resistance. (Kuranovas and Kvedaras 2007)

This study investigates the behavior of a special type of composite sections, a steel reinforced concrete column with GFRP control bars. This structural component can be used for relocating the plastic hinge region particularly in seismic zones.

During strong earthquakes, plastic hinges form at the ends of bridge columns. This plastic hinge formation causes yield penetration of the column longitudinal reinforcement into the joint and may damage the foundation supporting the column. Post-earthquake retrofit of the damaged regions with bars suffering yield penetration is difficult and expensive (Cheng and Mander 1997). Therefore, it is desirable to force the development of plastic hinges away from the column foundation connection region. Fig. 1 demonstrates the location of plastic hinge formation in

*Corresponding author, Associate Professor, E-mail: rsabouta@syr.edu

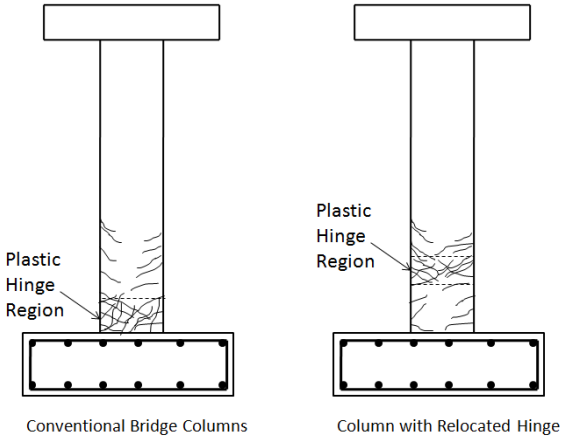

Fig. 1 Hinge formation in a typical bridge column and a column with relocated hinge

conventional bridge columns and the column designed with relocated plastic hinges.

Few studies have been conducted to relocate the plastic hinge regions from the column-footing joint in reinforced concrete bridge columns. One of these studies was done by Hose *et al.* (1997). This study recommended a design technique for relocating the plastic hinge in bridge columns away from the footing and increasing the capacity at the joint's interface by adding an inner concentric reinforcing cage within this end region. The analytical and experimental results indicated that this method successfully reduced the yield penetration and consequential joint damage. However, additional transverse reinforcement for columns is needed in order to provide adequate confinement and ductility.

Shifting the plastic hinge away from the footing is desirable to reduce the yield penetration into the joint and avoid complex detailing in a congested region of the structure. However, relocating the plastic hinge should not be too far from the joint region for two reasons. First, increasing the flexural ductility will form large flexural -shear cracks which result in a loss of shear capacity. Second, the effective height of the column is reduced making the influence of shear on the hinge region more critical. Thus, relocating the plastic hinge region should be done in a way that prevents yield penetration into the footing without significantly increasing the shear demand (Priestley *et al.* 1994, Hose *et al.* 1997).

The bond behavior between the GFRP reinforcement and concrete is different from that of steel reinforcing bars since various key parameters that influence bond performance are different, such as lower modulus of elasticity and surface deformations. The bond mechanism between the GFRP bars and concrete has been studied widely by many researchers. From experimental results it was observed that the bond between GFRP reinforcement and concrete depends on several factors, such as the surface condition of the bar, embedment length, bar diameter, concrete cover, spacing between the bars, concrete compressive strength, chemical bonding and environmental agents (Soong *et al.* 2011, Baena *et al.* 2009, Pecce *et al*. 2001, Tighiouart *et al.* 1998, Harajli and Abouniaj 2010, Ehsani *et al.* 1996, Galati *et al.* 2005, Muñoz 2010).

The local bond stress can be expressed generally in Eq. (1). From this equation, we can observe that for the same bar diameter and strain level in the control bars, GFRP exhibits lower bond stress than steel. As a result, the use of these bars could potentially cause significantly less damage to the column's concrete core during a seismic event. Fig. 2 shows the locations of plastic hinge

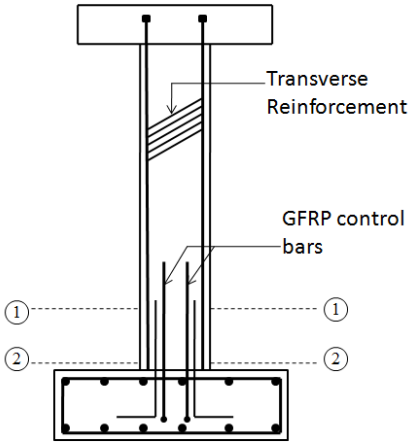

Fig. 2 Typical details of bridge pier with GFRP control bars (Not all bars are shown for clarity)

formation in a typical bridge pier with GFRP control bars. The plastic hinge would form near Section 1-1 in a splice-free region, instead of Section 2-2, thus the shifted plastic hinge will exhibit higher strength and ductility (Aboutaha *et al.* 2011).

$$\tau = \frac{D_g \times E_g}{4} \frac{d\varepsilon_g}{dx} \tag{1}$$

In Eq. (1), τ is the average bond stress; D_g is the diameter of GFRP bars; E_g is the elastic modulus of GFRP bars and $\frac{d\varepsilon_g}{dx}$ is the slope of the strain distribution curve.

2. Simulation model

The behavior of steel reinforced concrete columns with GFRP control bars is studied by analytical investigations. Numerical analyses were conducted using coding with MATLAB© software to obtain the full nominal interaction M-P curves for any hybrid circular reinforced concrete member. The code is modeled to account for appropriate constitutive material models. Also, it is refined in such a way where the user would input the cross section dimensions and material properties of the section desired for analysis. Furthermore, the user can specify the desired increment to plot the interaction diagram. The key to this code is to monitor the depth of concrete compressive zone "*x*" through increments. For this study, 5.08 mm (0.2 inches) increment is used for better accuracy.

3. Materials constitutive model

The materials used in the analysis involved steel reinforcing bars, GFRP bars and concrete. First, the steel reinforcement used is assumed to have the yielding stress of 414 MPa (60 Ksi), while its elastic modulus is considered to be 200 GPa (29,000 Ksi). The stress strain curve of the

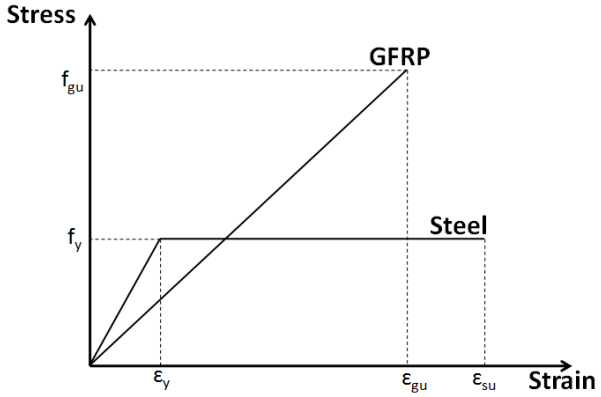

Fig. 3 Idealized stress-strain curves for steel and GFRP materials

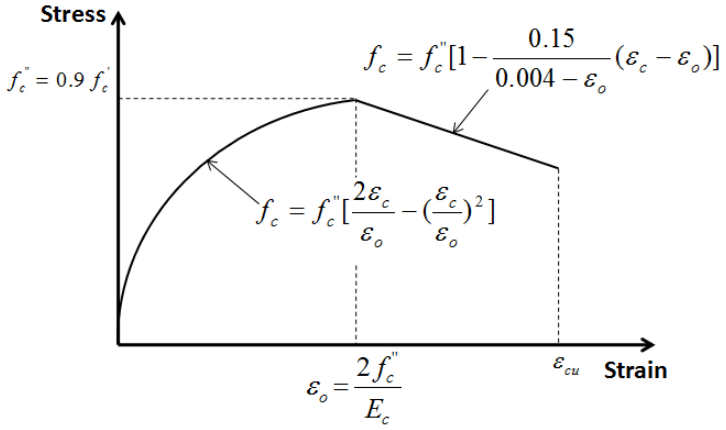

Fig. 4 Compressive stress -strain relation of concrete

reinforcing bars is assumed to be elastic perfectly plastic. Second, GFRP bar has elastic to failure property, with ultimate tensile strength of 1200 MPa (175 Ksi), and ultimate strain of 2%. All the material properties for the GFRP bars were obtained from the technical information by the manufacturer and tested by Aboutaha (2005). GFRP compressive strength was neglected in the analysis. Idealized stress-strain curves for constitutive steel and GFRP materials are shown in Fig. 3.

Third, normal weight concrete with uniaxial compressive strength ranged from 27.6 MPa (4000 Psi) to 68.9 MPa (10,000 Psi) was chosen for this study. Concrete tensile strength was neglected. The compressive stress-strain relation of concrete is shown in Fig. 4 (Wight and MacGregor 2008) and it can be described by

$$f_c = \begin{cases} f_c^{"}\left[\dfrac{2\varepsilon_c}{\varepsilon_o} - \left(\dfrac{\varepsilon_c}{\varepsilon_o}\right)^2\right] & for\ \ \varepsilon_c \le \varepsilon_o \\ f_c^{"}\left[1 - \dfrac{0.15}{0.004 - \varepsilon_o}(\varepsilon_c - \varepsilon_o)\right] & for\ \ \varepsilon_c \le \varepsilon \end{cases} \tag{2}$$

$$f_c'' = 0.9 f_c' \tag{3}$$

$$\varepsilon_o = \frac{2 f_c''}{E_c} \tag{4}$$

In Eq. (2), f_c is the compressive stress at i^{th} layer when the concrete section is discretized into layers; f_c' is the concrete confined compressive stress; f_c'' is the concrete compressive stress at strain ε_0 given in Eq. (3) ; ε_c is the strain at f_c compressive stress; ε_o is the strain at the peak compressive stress given in Eq. (4) and E_c is the modulus of elasticity of the concrete.

4. Construction of hybrid M-P interaction curves

The analysis of the hybrid steel-GFRP columns is equivalent to that of conventional steel reinforced concrete columns with the primary difference being the use of elastic to failure GFRP control bars. The main purpose for these bars is the relocation of the plastic hinge region. The following assumptions were considered while constructing the M-P curves:

• Plane section before loading remains plane after loading (strain in the concrete, steel and GFRP reinforcement is proportional to the distance from the neutral axis) ;

• The maximum usable compressive strain in concrete is assumed to be 0.003;

• The tensile strength of concrete is neglected;

• The GFRP compressive strength is also neglected;

• The elastic modulus of steel *Es*= 200 GPa (29,000 Ksi). Beyond yielding, *Es*=0;

• The tensile behavior of the GFRP bars is linearly elastic to failure;

• The column was transversely reinforced according to AASHTO LRFD bridge design specifications;

• The details of the transverse reinforcement were assumed to have adequate strength to confine the plastic hinge region and they were not investigated in this study and

• Perfect bonding is assumed between steel, GFRP and concrete.

M-P interaction diagram presents the envelope of the nominal capacity of the column section under various axial loads and moments. Some points in this diagram have special characteristics as shown in Fig. 5:

X_c : Strain distribution corresponding to uniform pure axial compressive strain of concrete (ε_{cu} =0.003)

X_b : Strain distribution corresponding to the balanced failure with a maximum compressive strain of concrete and yielding tensile strain at the extreme tension layer of steel reinforcement

X_m : Strain distribution corresponding to the pure bending moment and zero axial force

X_t : Strain Distribution corresponding to the pure axial tension

X_g : Strain distribution corresponding to the limiting fracture failure at the extreme tension layer

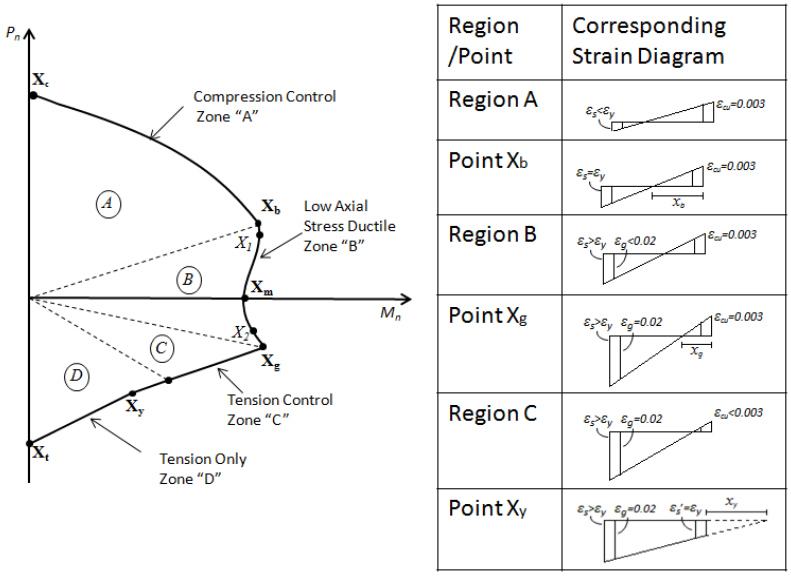

Region /Point	Corresponding Strain Diagram
Region A	$\varepsilon_s<\varepsilon_y$ $\varepsilon_{cu}=0.003$
Point Xb	$\varepsilon_s=\varepsilon_y$ $\varepsilon_{cu}=0.003$ x_b
Region B	$\varepsilon_s>\varepsilon_y$ $\varepsilon_g<0.02$ $\varepsilon_{cu}=0.003$
Point Xg	$\varepsilon_s>\varepsilon_y$ $\varepsilon_g=0.02$ $\varepsilon_{cu}=0.003$ x_g
Region C	$\varepsilon_s>\varepsilon_y$ $\varepsilon_g=0.02$ $\varepsilon_{cu}<0.003$
Point Xy	$\varepsilon_s>\varepsilon_y$ $\varepsilon_g=0.02$ $\varepsilon_s'=\varepsilon_y$ x_y

Fig. 5 General hybrid steel-GFRP interaction diagram

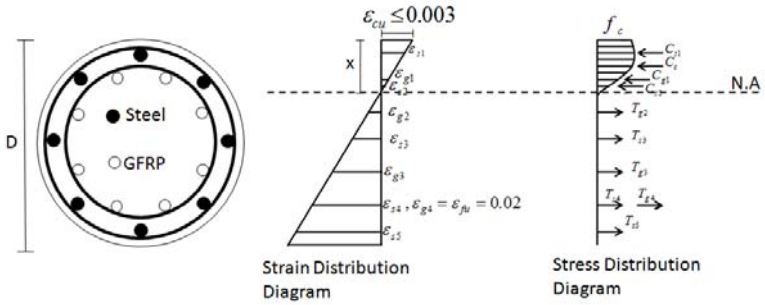

Fig. 6 Strain and stress distribution diagram used to construct the nominal M-P interaction diagrams

of GFRP, having a maximum compressive strain of concrete

X_y : Strain distribution corresponding to the point where all steel bars in the section yields

Strain compatibility approach, equilibrium principle and constitutive laws were adopted to construct the nominal M-P interaction curve for any column cross section. In the source code, the strain in the concrete, steel and GFRP reinforcement is proportional to the distance from the neutral axis as shown in Fig. 6. The axial load P was calculated using the equilibrium equation, while the internal moment M was calculated by summing the moments of all internal forces about the plastic centriod. The compression force in the concrete is evaluated by the integral of the stress over the area above the neutral axis. Stresses in the steel and GFRP bars were calculated as follows

$$\text{Steel Stress in Tension} \qquad f_s = E_s \times \varepsilon_s \le f_y \tag{5}$$

$$\text{Steel Stress in Compression} \qquad f_s = (E_s \times \varepsilon_s - f_{ccs}) \le (f_y - f_{ccs}) \tag{6}$$

GFRPStress in Tension $f_g = E_g \times \varepsilon_g \leq f_{gu}$ (7)

In Eqs. (5)-(7), f_s and f_g are the stress in steel and GFRP respectively; E_s and E_g are the modulus of elasticity of steel and GFRP respectively; ε_s and ε_g are the strain in steel and GFRP respectively; f_y is the yield strength of steel; f_{ccs} is the stress in concrete at the level of the compression steel estimated using Eq. 2; and f_{gu} is the ultimate tensile strength of GFRP bars.

5. Discussion of hybrid M-P interaction curves

The hybrid M-P interaction diagram can be divided into four zones as follows: (1) Compression control zone "*A*", (2) Low axial stress ductile zone "*B*", (3) Tension control zone "*C*" and (4) Tension only zone "*D*", as shown in Fig. 5.

The compression control zone "*A*", starts from the balance failure point (X_b) and ends at the pure axial compression point (X_c). In this zone the maximum concrete strain is 0.003. The steel in this region remains elastic (except at point X_b), and the GFRP was assumed not to carry any compressive stresses. Furthermore, as any typical steel reinforced concrete interaction diagram, the failure mechanism in the compression control zone would be governed by crushing of the concrete at the extreme compression fiber.

Low axial stress ductile Zone "*B*" starts from the balance point (X_b) and ends at the fracture GFRP limit point (X_g). In this zone, the steel yields and the strain in GFRP is less than the ultimate limit fracture of 0.02 except point (X_g). Meanwhile, the mode of failure starts with yielding of the steel bars followed by crushing of the concrete which is a typical ductile failure response.

In the tension control zone "*C*", where the mode of failure is controlled by fracture of the GFRP bars, the strain in the extreme tension layer of GFRP control bars is fixed to its ultimate limit 0.02. Although the mode of failure is controlled by fracture of GFRP bars, the mode of failure is considered ductile since the GFRP are control bars while the steel are primary ones.

In zone "*D*", the contribution of concrete in tension was neglected everywhere. Like in zone *C*, the strain in the extreme tension layer of GFRP is still fixed as its ultimate limit of 0.02. In zone "*D*", the failure starts with yielding of steel, followed by fracture of the GFRP control bars. It's noticeable that the behavior of the M-P diagram in this zone is approximately linear and the slope of the curve is changing after yielding of each layer of steel bars. This is due to the fact that after the steel yields, the steel bars lose their stiffness and their force remains constant, while the elastic to failure GFRP bars dominate the section stiffness.

The hybrid steel-GFRP concrete sections show a second discontinuity point X_g in their moment axial interaction diagrams. This behavior reflects a condition where the maximum strain in GFRP reaches its ultimate. Moreover, the linear elastic to failure GFRP material forms a *z*-shape in the interaction diagrams (inflection points X_1 and X_2 shown in Fig. 5).This shape is a mathematical reflection of the combination of concrete, steel and GFRP behaviors in the hybrid section.

In order to locate the inflection points of the z-shaped curve, the following procedure was used. First, the column moment capacity equation was written in terms of "*x*", the depth of the concrete compression zone. Then, the first derivative of this equation with respect to "*x*" is obtained and

solved. The resulting roots of this derivative constitute a set of potential inflection points. Valid ones should match the following two criteria. The first inflection point should be located at or near the balance condition point since the GFRP forces would be lower than that of steel in this region. The second criterion of the inflection point is that it should be at or near X_g , and caused by GFRP since in this region the forces in GFRP will be higher than that of steel.

6. Results and discussions

In order to investigate the effectiveness of using GFRP control bars for shifting the plastic hinge region, several circular column sections were considered. The primary reference column was 1828.8 mm (72 inches) in diameter. It was designed and transversely detailed according to the current AASHTO LRFD bridge design specifications (AASHTO 2010). The longitudinal steel reinforcement ratio ρ_s (area of steel/gross area of concrete) of 1.25% was selected, which is equivalent to 40 32 mm (40#10). The details of the transverse reinforcement were assumed to have adequate capacity to confine the plastic hinge regions following the AASHTO bridge design specifications. Therefore, they were not investigated in this study. Fig. 7 shows details of the reference column sections.

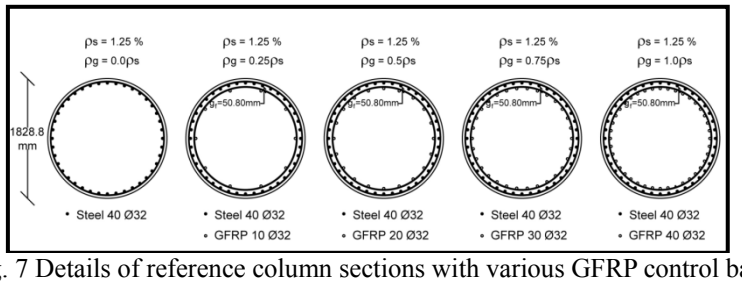

Fig. 7 Details of reference column sections with various GFRP control bars

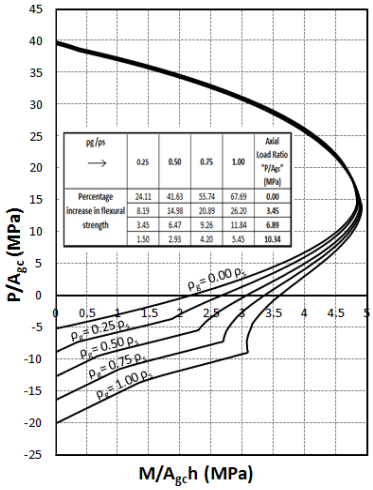

Fig. 8 Non-dimensional interaction diagrams for the reference column by varying ρ_g (f_c'=41.4 MPa, f_y=414 MPa, g_f=50.8 mm and ρ_s=1.25%)

Fig. 8 shows the nominal non-dimensional M-P interaction diagrams for the reference column. The main variable in this series is the amount of GFRP control bars. Several amounts of GFRP bars were considered, which had 10, 20, 30, or 40 ϕ 32 mm (# 10), corresponding to GFRP ratio ρ_g (area of GFRP/ gross area of concrete) as 0.25 ρ_g , 0.5 ρ_g , 0.75 ρ_g and 1.00 ρ_g . The GFRP bars were located at 50.8 mm (2 inches) measured from the main steel bars g_f . This value was used since it is the most practical distance, and offers the longest moment arm for the GFRP bars. For this specific set of curves, the concrete compressive strength was 41.4 MPa (6000 Psi) and the steel yield strength was 414 MPa (60 Ksi).

From these curves it was observed that for any specific axial stress, an increase in the amount of GFRP control bars would lead to an increase in the bending moment capacity of the column section. However, as the axial stress increases, the rate of increase in the bending capacity decreases. We can also notice that in the compression control zone, all the hybrid curves almost coincide with the steel reinforced concrete column's curve, since GFRP was assumed not to carry compressive stresses. Thus, GFRP bars are not efficient in increasing the bending resistance of the column section under high compressive axial stress (compression control zone A).

In addition to the GFRP reinforcement ratio, its modulus of elasticity also plays a major role in the behavior of the interaction diagram. Fig. 9 shows the M-P interaction diagram for the reference column by varying the GFRP modulus of elasticity. The graph shows that the higher the modulus of elasticity, the higher the increase in the bending moment capacity.

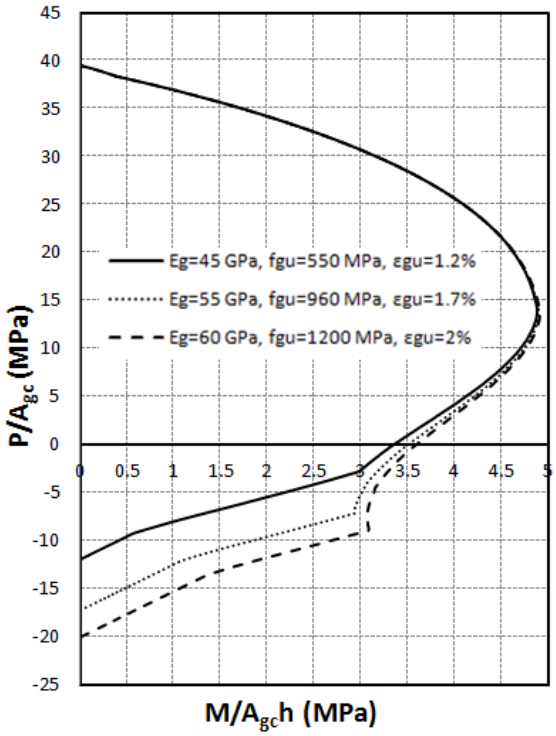

Fig. 9 Non-dimensional interaction diagrams for the reference column by varying GFRP properties (f_c'=41.4 MPa, f_y =414 MPa, g_f=50.8 mm, ρ_s=1.25% and ρ_g= ρ_s)

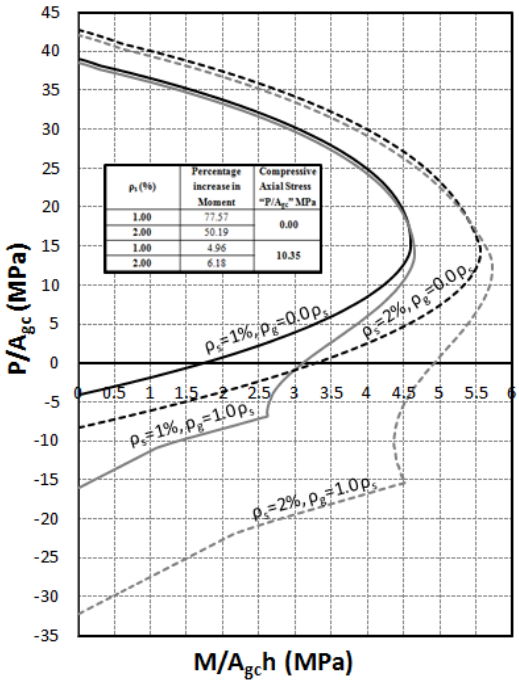

ρ_s (%)	Percentage increase in Moment	Compressive Axial Stress "P/A_{gc}" MPa
1.00	77.57	0.00
2.00	50.19	
1.00	4.96	10.35
2.00	6.18	

Fig. 10 Non-dimensional interaction diagrams for the reference column by varying ρ_s and ρ_g (f_c'=41.4 MPa, f_y=414 MPa and g_f=50.80 mm)

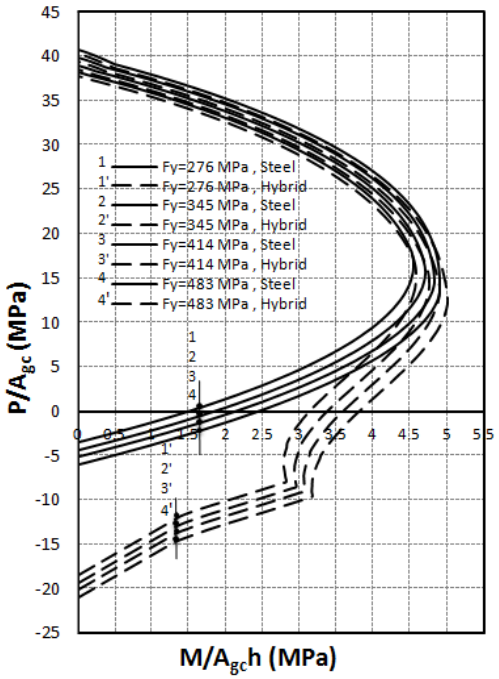

Fig. 11 Non-dimensional interaction diagrams for the reference column by varying f_y (f_c'=41.4 MPa, g_f=50.8 mm, ρ_s=1.25% and ρ_g= ρ_s)

The combined effect of simultaneously varying the steel and the GFRP reinforcement is shown in Fig. 10. The results show that increasing the steel ratio would decrease the percentage increase in the enhanced moment capacity at low axial stress. For example, at the pure bending moment (zero axial stress), the effect of doubling the reinforcement ratio ρ_s from 1% to 2% with ratio (ρ_g / ρ_s) equal to 1 decreases the percentage increase in flexural strength from 77.57 to 50.19. At high axial stress, steel ratio has insignificant effect.

Fig. 11 shows the M-P interaction diagram for the reference column by varying the steel yield strength from 276 MPa (40 ksi) to 483 MPa (70 Ksi). The results show that the steel yield strength has the same effect on the increase in flexural strength as the reinforcement ratio. Increasing the yield strength would decrease the percentage increase in flexural strength at low axial stress, and there is no significant effect at higher axial stress.

Furthermore, the effect of the concrete compressive strength f_c' on the GFRP-steel sections was also investigated as shown in Fig. 12. We can notice that f'_c has a positive effect on increasing flexural strength particularly at low axial stresses.

In addition to the reinforcement and material properties, column cross sectional area was also investigated represented by γ (the ratio of the distance between centers of longitudinal steel reinforcement in the outer layers to the column diameter). Fig. 13 illustrates the influence of the cross sectional area on the hybrid steel-GFRP column. Five circular column cross sections were considered in this study, which had diameter of 609.6, 1219.2, 1828.8, 2438.4 and 3048 mm (2, 4, 6, 8 and 10 ft) corresponding to γ ratio as 0.78, 0.89, 0.93, 0.95, and 0.96 respectively. The results indicate that column cross section has a large influence on the flexural capacity of the reinforced

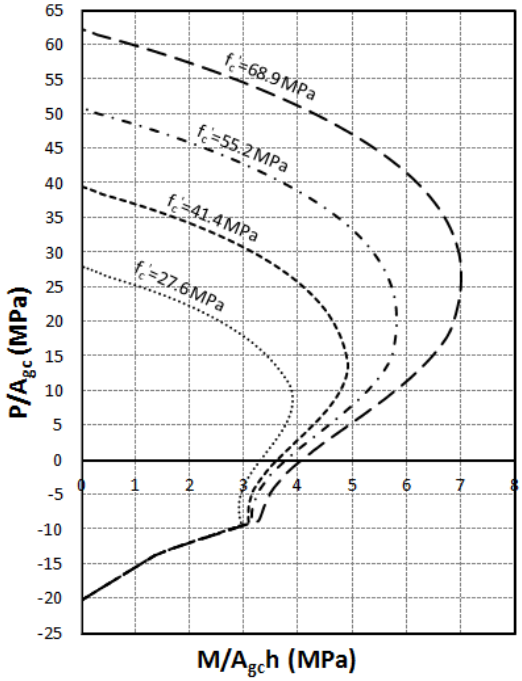

Fig. 12 Non-dimensional interaction diagrams for the reference column by varying f_c' (f_y=414 MPa, g_f=50.8 mm, ρ_s=1.25% and ρ_g=ρ_s)

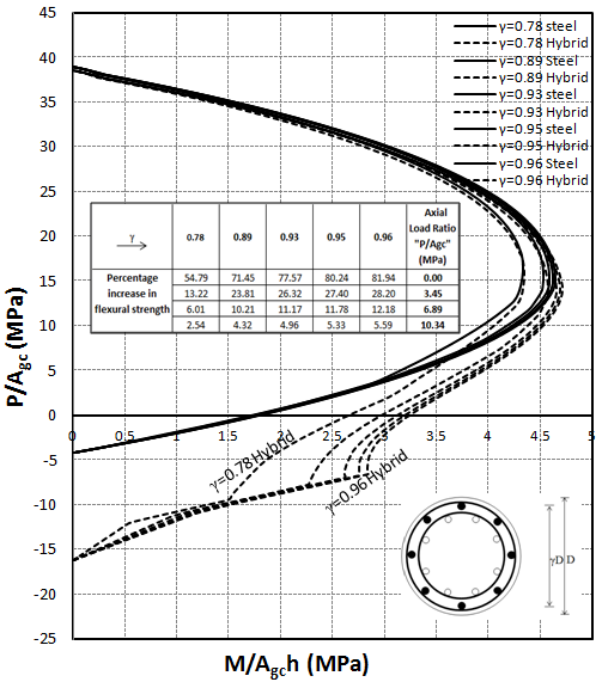

γ	0.78	0.89	0.93	0.95	0.96	Axial Load Ratio "P/Agc" (MPa)
Percentage increase in flexural strength	54.79	71.45	77.57	80.24	81.94	0.00
	13.22	23.81	26.32	27.40	28.20	3.45
	6.01	10.21	11.17	11.78	12.18	6.89
	2.54	4.32	4.96	5.33	5.59	10.34

Fig. 13 Non-dimensional interaction diagrams by varying γ (f_c'=41.4 MPa, f_y =414 MPa, g_f=50.8 mm ρ_s=1.0%, ρ_g= ρ_s)

Table 1 Ductility of steel-GFRP sections versus steel-steel sections for the reference column at pure moment

ρ_g/ρ_s or ρ_s'/ρ_s	Steel-GFRP section	Steel-Steel section
0.00	5.86	5.86
0.25	5.03	5.09
0.50	4.54	4.53
0.75	4.19	4.15
1.00	3.93	3.85

Where:

ρ_g = is the ratio of the total amount of GFRP control bars A_g to the gross area of the column A_{gc}

ρ_s' = is the ratio of the total amount of steel control bars A_s' to the gross area of the column section A_{gc}

ρ_s = is the ratio of the total amount of primary steel bars A_s to the gross area of the column section A_{gc}

concrete column with GFRP control bars. Under any specific axial stress, an increase in the column cross section leads to an increase in the enhanced bending strength.

Finally, it is often necessary to determine the ductility of a given column which reflects the ability to sustain inelastic deformations before collapse without substantial loss of strength. The ductility was defined as the ratio of curvature at ultimate load to the curvature at first yield. Table 1 shows the ductility of the hybrid steel-GFRP sections versus the steel-steel sections of the

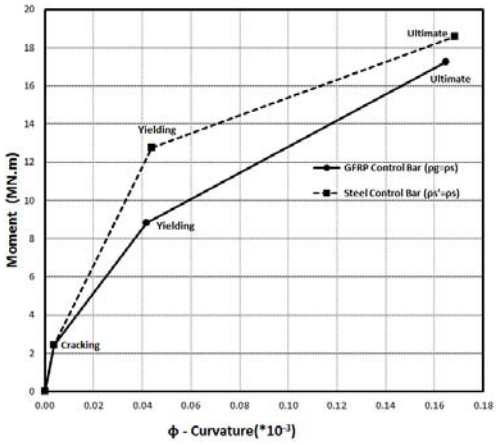

Fig. 14 M-ϕ diagram for GFRP versus steel control bar for the reference column section at pure axial moment

reference column and Fig. 14 shows the moment curvature M-ϕ diagram for GFRP versus steel control bar at pure axial moment. The results indicate that steel-GFRP sections have good ductility and are relatively equal to those of conventional reinforced steel column sections. Moreover, it should be noted here that the hybrid sections confine the concrete with two steel cages causing the concrete to be under a triaxial stress state. This state can attain higher compressive strength and higher ultimate strain resulting in larger deformation ability, which is an important criterion for seismic performance of columns.

7. Conclusions

This paper presents results of an analytical investigation of the behavior of composite steel reinforced concrete circular column with GFRP control bars. Based on the results of this investigation, the following conclusions are drawn:

1. GFRP control bars are effective in increasing the bending capacity of steel reinforced concrete sections subject to low axial loads around or below 15% of its ultimate pure axial stress.
2. An increase in the amount of GFRP bars leads to an increase in the bending capacity of the column section, while the rate of increase in the bending capacity decreases as the axial stress increases.
3. The higher the modulus of elasticity of the GFRP control bars, the higher the increase in the enhanced bending moment capacity.
4. At low axial stress, an increase in the steel reinforcement ratio or its yield strength would lead to a decrease in the enhanced bending moment capacity. However, increasing these variables has insignificant effect at higher axial stresses.
5. The larger the columns cross sections, the higher the increase in the bending strength.
6. Since the compressive strength of GFRP is small, GFRP control bars are not effective in increasing the bending capacity of steel reinforced concrete sections subject to high axial stress (generally greater than 10 MPa).
7. GFRP control bar is superior to a steel auxiliary control bar, since it develops lower bond stress

with the surrounding concrete which causes less damage to the concrete core during frequent seismic events.

It is concluded that a steel-GFRP concrete column exhibits adequate structural performance through high strength and adequate ductility. Therefore, it has the ability to relocate the plastic hinge region far from the footing-column joint region, which makes this composite section a viable alternative for the application in bridges located in seismic zones. Recommended future research should involve experimental investigation of full scale steel-GFRP reinforced concrete columns.

References

AASHTO LRFD (2010), "Bridge design specifications", American association of state highway and transportation officials, Washington, DC.

Aboutaha, R.S., El-Helou, R.G. and Shraideh, M.S. (2011), "Seismic control of plastic mechanism of steel reinforced concrete columns by the use of GFRP bars", *Proceedings of the Third Asia-Pacific Conference on FRP in Structures*, APFIS 2012, Hokkaido University, Sapporo, Japan.

Aboutaha, R.S. (2005), *Investigation of mechanical properties of ComBAR®*, Research Report, Syracuse University, NY.

Baena, M., Torres, L. and Barris, C. (2009), "Experimental study of bond behavior between concrete and FRP bars using a pull-out test", *Compos*., **40**, 784-798.

Cheng, C.T. and Mander, J.B. (1997), "Seismic design of bridge columns based on control and reparability of damage", Technical Report NCEER-97-0013, University of Buffalo, NY.

Ehsani, M.R., Saadatmanesh, H. and Tao, S. (1996), "Design recommendations for bond of GFRP rebars to concrete", *J. Struct. Eng.-ASCE*, **122**(3), 247-254.

Galati, N., Nanni, A., Dharani, L.R., Focacci, F. and Aiello, M.A. (2006), "Thermal effects on bond between FRP rebars and concrete", *Compos*., **37**, 1223-1230.

Harajli, M. and Abouniaj, M. (2010), "Bond performance of GFRP bars in tension: Experimental evaluation and assessment of ACI 440 guidelines", *J. Comput. Constr.-ASCE*, **14**(6), 659-668.

Hose, Y.D., Seible, F. and Priestley, M.J.N. (1997), "Strategic relocation of plastic hinges in bridge columns", Report No.SSRP-97/05, University of California, San Diego, CA.

Kuranovas, A. and Kvedaras, A.K. (2007), "Behavior of hollow concrete–filled steel tubular composite elements", *J. Civil Eng. Manage*, **13**(2), 131-141.

MATLAB© (2011), *Math works*, http://www.mathworks.com/products/matlab/

Muñoz, M. (2010), "Study of bond behavior between FRP reinforcement and concrete", PhD. thesis, University of Girona, Spain.

Peece, M., Manfredi, G., Realfonzo, R. and Cosenza, E. (2001), "Experimental and analytical evaluation of bond properties of GFRP bars", *J. Mater. Civil Eng*., **13**(4), 282-290.

Priestley, M., Verma, R. and Xiao, Y. (1994), "Seismic shear strength of reinforced concrete columns", *J. Struct. Eng.-ASCE*, **120**(8), 2310-2329.

Soong, W.H., Raghavan, J. and Rizkalla, S. (2011), "Fundamental mechanisms of bonding of glass fiber reinforced polymer reinforcement to concrete", *Constr. Build. Mater*., **25**(6), 2813-2821.

Tighiouart, B., Benmokraneu, B. and Gao, D. (1998), "Investigation of bond in concrete member with fiber reinforced Polymer bars", *Constr. Build. Mater*., **12**(8), 453-462.

Wight, J. and MacGregor, J. (2008), *Reinforced concrete mechanics and design*, Prentice-Hall, New Jersey.

CM